Elsevier Editorial System(tm) for Journal of Colloid and Interface Science
Manuscript Draft

Manuscript Number:

Title: Reducing the size of gold nanostars does not increase internalization in SH-SY5Y cells

Article Type: Full length article

Section/Category: E. Biomaterials and Nanomedicine

Keywords: nanostars; nanoparticles; gold; cell internalization

Corresponding Author: Dr. Giacomo Dacarro, Ph.D.

Corresponding Author's Institution: Università degli Studi di Pavia

First Author: Giacomo Dacarro, Ph.D.

Order of Authors: Giacomo Dacarro, Ph.D.; Piersandro Pallavicini; Serena M Bertani; Giuseppe Chirico; Laura D'Alfonso; Andrea Falqui; Nicoletta Marchesi; Alessia Pascale; Laura Sironi; Angelo Taglietti; Efisio Zuddas

Abstract: The synthesis of large pentatwinned five-branched gold nanostars (GNS) has been modified so to obtain overall dimensions shrunk to 60% and a lower branches aspect ratio, leading to a dramatic blue shift of their two near-infrared (NIR) localized surface plasmon resonances (LSPR) absorptions but still maintaining one LSPR in the biotransparent NIR range. The interactions of polyethylene glycol (PEG) coated large and shrunk GNS with SH-SY5Y cells revealed that the large ones (DCI - diameter of the circumference in which GNS can be inscribed = 76 nm) are internalized more efficiently than the shrunk ones (DCI = 46 nm), correlating with a decreased cells surving fraction.

Suggested Reviewers: Thorfinnur Gunnlaugsson Prof.
School of Chemistry, Trinity College, Dublin, Ireland
gunnlaut@tcd.ie

Paula M Mendes Prof.
School of Chemical Engineering, University of Birmingham
p.m.mendes@bham.ac.uk

Miguel Vazquez Lopez Prof.
Department of Inorganic Chemistry, University of Santiago de Compostela
miguel.vazquez.lopez@usc.es

Lucia Pasquato Prof.
Department of Chemical Sciences, University of Trieste
lpasquato@units.it

Diego Tesauro Prof.
Department of Pharmaceutical Sciences, University of Naples
diego.tesauro@unina.it

Dear Editor,
please consider this manuscript for publication in Journal of Colloid and Interface Science as a *full paper*.

We present here the synthesis of five-branched symmetrical gold nanostars whose overall dimensions are shrunk to the half of the large ones (80 nm) already described by us in the literature.
The synthetic rationale is:
a) to try to find a synthetic approach that produces such nanostars with dimensions smaller than the "golden threshold" of 50 nm, that literature suggests as the optimal for cell internalization.
b) to keep the optical and physical-chemical features of the shrunk nanostars as interesting as those of their larger relatives.
We illustrate in this paper how we succeeded in both goals, completing the study with spectroscopic, TEM and HR-TEM studies that allows to propose a mechanism for gold nanostars growth and for the variation of their properties connected with dimensions and shape.
Moreover, the internalization of both large and shrunk gold nanostars were studied in a model cell line (human neuroblastoma SH-SY5Y). Surprisingly we found that the larger nanostars are internalized better than the small ones, this adding a further confirmation to the sparse observations found in the literature that changing the shape of a given nanoparticle also changes the dimensional range that promotes its cellular uptake. We indicate here that the 50 nm "golden threshold" is surely valid, but only for spherical gold nanoparticles.

I believe that this paper meets the high standards of novelty and interest for the wide audience of JCIS, as it presents a synthetic shrinking approach that may be valid for all seed-growth syntheses. Moreover, the experimental demonstration that nanostars that are "large" in the nanochemical community perception enter cells better than smaller ones adds important informations to the drug delivery and therapeutical techniques based on nanoparticles. Finally, the synthetic approach and the chemical and chemical physical characterization of the species presented in this paper have the typical "style" of JCIS, with a solid inorganic chemistry background joined by many other chemical areas such as nanochemistry, biochemistry, physical-chemical analysis, high resolution imaging.

ESI contains further data (*e.g.* TEM images, photothermal profiles, two-photon luminescence spectra), accurately mentioned in the main text at the proper place, in order to fully support our findings.

Kind regards

Dr. Giacomo Dacarro
Department of Chemistry
University of Pavia

*3: Graphical Abstract

Click here to download high resolution image

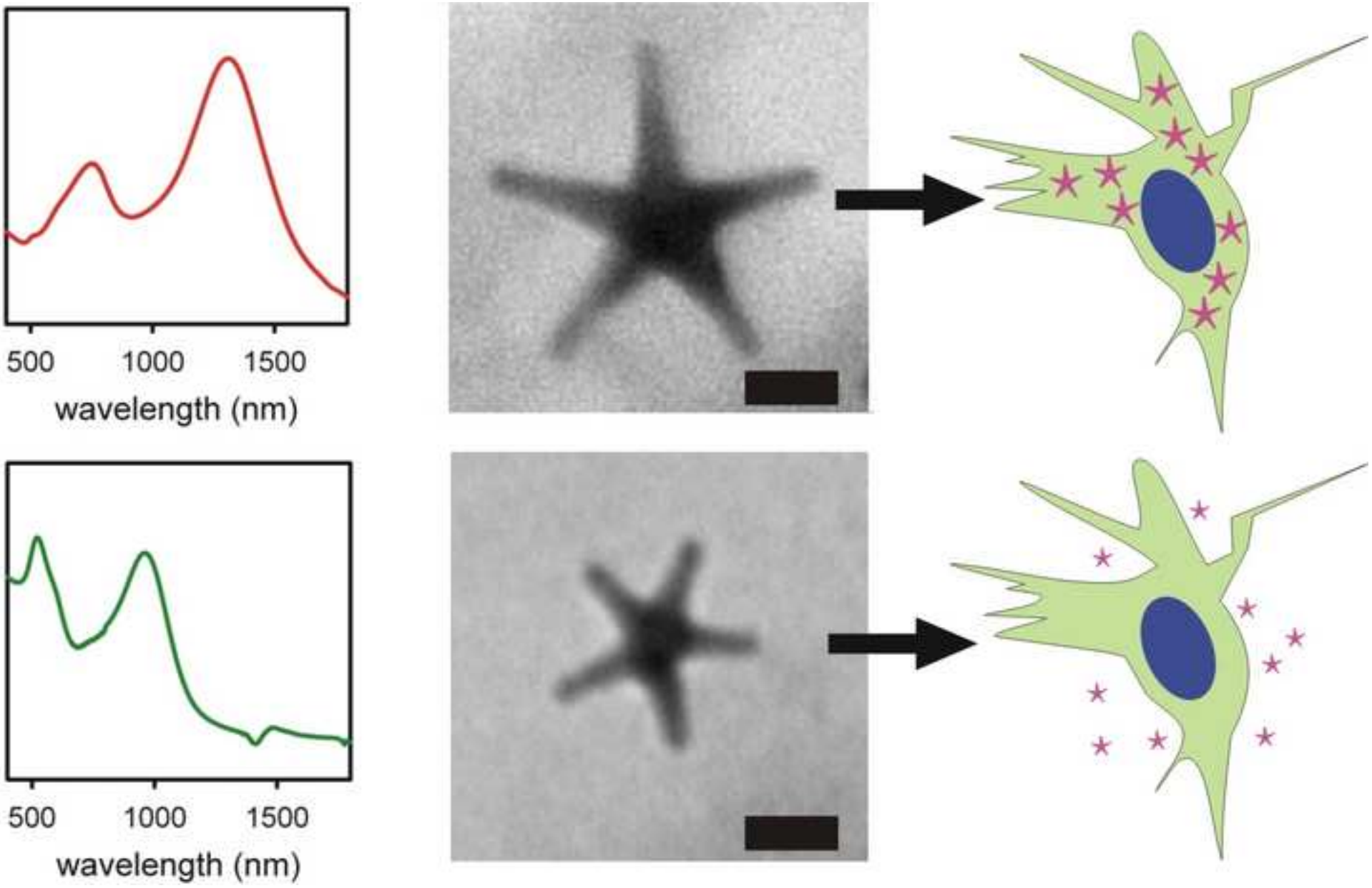

Reducing the size of gold nanostars does not increase internalization in SH-SY5Y cells

Giacomo Dacarro,*[a] Piersandro Pallavicini,*[a] Serena Maria Bertani,[a] Giuseppe Chirico,[b] Laura D'Alfonso,[b] Andrea Falqui,[c] Nicoletta Marchesi,[d] Alessia Pascale,[d] Laura Sironi,[b] Angelo Taglietti[a] and Efisio Zuddas[c]

[a]*Dipartimento di Chimica, Università degli Studi di Pavia, v.le Taramelli 12, 27100 Pavia -Italy. Email; giacomo.dacarro@unipv.it*, +39382987923; *piersandro.pallavicini@unipv.it*, +39283987336.
[b]*Dipartimento di Fisica G. Occhialini, Università degli Studi di Milano-Bicocca, Piazza della Scienza, 3, 20126 Milano*
[c]*King Abdullah University of Science and Technology (KAUST), Biological and Environmental Sciences and Engineering (BESE) Division, NABLA Lab, 23955-6900 Thuwal, Saudi Arabia.*
[d]*Dipartimento di Scienze del Farmaco, Sezione di Farmacologia, Università degli Studi di Pavia, v.le Taramelli 12, 27100 Pavia - Italy*

email addresses:

Giacomo Dacarro (giacomo.dacarro@unipv.it)
Piersandro Pallavicini (piersandro.pallavicini@unipv.it)
Serena Maria Bertani (serenabertani@libero.it)
Giuseppe Chirico (giuseppe.chirico@unimib.it)
Laura D'Alfonso (laura.dalfonso@unimib.it)
Andrea Falqui (andrea.falqui@kaust.edu.sa)
Nicoletta Marchesi (nicoletta.marchesi@unipv.it)
Alessia Pasacale (alessia.pascale@unipv.it)
Laura Sironi (laura.sironi@unimib.it)
Angelo Taglietti (angelo.taglietti@unipv.it)
Efisio Zuddas (efisio.zuddas@kaust.edu.sa)

Reducing the size of gold nanostars does not increase internalization in SH-SY5Y cells

Giacomo Dacarro,*[a] Piersandro Pallavicini,*[a] Serena Maria Bertani,[a] Giuseppe Chirico,[b] Laura D'Alfonso,[b] Andrea Falqui,[c] Nicoletta Marchesi,[d] Alessia Pascale,[d] Laura Sironi,[b] Angelo Taglietti[a] and Efisio Zuddas[c]

[a]*Dipartimento di Chimica, Università degli Studi di Pavia, v.le Taramelli 12, 27100 Pavia -Italy. Email; giacomo.dacarro@unipv.it*, +39382987923; *piersandro.pallavicini@unipv.it*, +39283987336.
[b]*Dipartimento di Fisica G. Occhialini, Università degli Studi di Milano-Bicocca, Piazza della Scienza, 3, 20126 Milano*
[c]*King Abdullah University of Science and Technology (KAUST), Biological and Environmental Sciences and Engineering (BESE) Division, NABLA Lab, 23955-6900 Thuwal, Saudi Arabia.*
[d]*Dipartimento di Scienze del Farmaco, Sezione di Farmacologia, Università degli Studi di Pavia, v.le Taramelli 12, 27100 Pavia - Italy*

Abstract

The synthesis of large pentatwinned five-branched gold nanostars (GNS) has been modified so to obtain overall dimensions shrunk to 60% and a lower branches aspect ratio, leading to a dramatic blue shift of their two near-infrared (NIR) localized surface plasmon resonances (LSPR) absorptions but still maintaining one LSPR in the biotransparent NIR range. The interactions of polyethylene glycol (PEG) coated large and shrunk GNS with SH-SY5Y cells revealed that the large ones (DCI - diameter of the circumference in which GNS can be inscribed = 76 nm) are internalized more efficiently than the shrunk ones (DCI = 46 nm), correlating with a decreased cells surving fraction.

Keywords: nanostars, nanoparticles, gold, cell internalization

Introduction

Gold nanostars (GNS) are gold nanoparticles with a core and a variable number of branches protruding from it, typically in a urchin-like shape.[1-11] Some years ago we have introduced seed-growth syntheses of GNS that use surfactants weakly interacting with the Au surface as directing agents. These are the zwitterionic laurylsulphobetaine[12-13] (LSB) and non-ionic TritonX-100 (TX100).[14] From these syntheses nice regular shapes are obtained, with GNS featuring 4-6 sharp branches, a valuable feature for optical[15] and SERS[16] sensing. Moreover, GNS from LSB and from TX100 have one or two localized surface plasmon resonances (LSPR), respectively, placed in the near-infrared (NIR) region, that display an efficient photothermal response.[13-14] In addition, the absorption maxima of these LSPR bands are finely tunable in large wavelength ranges (750-1800 nm), in virtue of the tunability of the aspect ratio of the branches with synthetic conditions. This makes the absorption of such GNS able to match different laser sources. Finally, GNS from LSB and TX100 emit a strong luminescence when excited with the two-photon technique on their LSPR bands[15] and offer straightforward surface functionalization protocols, thanks to the easy replacement of the LSB or TX-100 surfactants weakly adhering to the Au surface. All these features make such particles interesting for a range of bio-medical applications, including in-vivo imaging[17] and photothermal therapy.[18-19]
Large quantities of surfactants are required for GNS syntheses, that are typically carried out in 0.1-0.4M LSB or TX100.

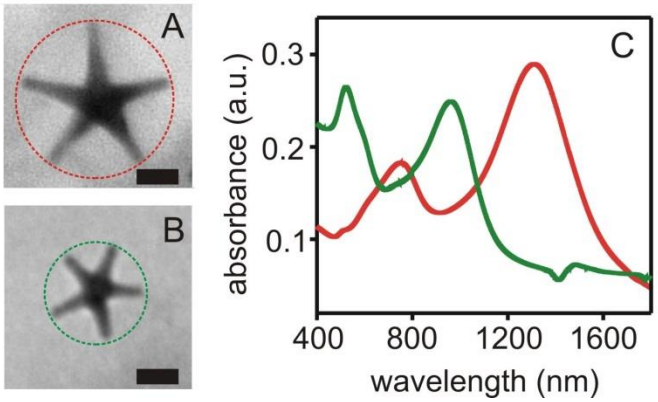

Figure 1. A: TEM image of a l-GNS (large GNS) from TX100 obtained with already published synthesis, DCI = 75nm.[R] **B**: TEM image of a s-GNS (shrunk GNS) prepared in this work, DCI = 45 nm. Dimensional bars are 20 nm. Dashed circles guide the eye to visualize DCI. **C**: absorption spectra. Red line: l-GNS. Green line: s-GNS

The latter surfactant has the additional advantage of a much lower cost with respect to LSB, and this has recently pushed us to focus on GNS obtained from such inexpensive reagent. GNS from TX-100 have relatively large dimensions. They have a regular, flat, 5-branched shape, allowing to define their dimensions with the diameter of the circumference in which they can be inscribed (DCI). The DCI of the GNS synthesized in our previous works varied from 70 to 100 nm, depending on synthetic conditions.[14] Figure 1A shows an example of those GNS at the minimum attainable dimensions,[14] and the corresponding absorption spectrum is displayed in Figure 1C(red). The spectrum shows the typical two NIR LSPR profile of GNS from TX100, with a 'long' band at ~1300 nm, an 'intermediate' band at ~ 750 nm, plus a 'short' band (of almost negligible intensity) at ~520 nm. While the latter is due to the transversal resonant oscillation of the valence electrons of the branches (and to some small spherical by-products), the 'intermediate' and 'long' bands were assigned to resonant longitudinal electrons oscillations along isolated branches ('intermediate' band) and collinear branches ('long' band),[14,20] with a phenomenon similar to what is observed when gold nanoparticles aggregate and form elongated objects.[21,22] The 'intermediate' and 'long' band positions fall in the biotransparent window of the NIR (750-900 nm[23]) and at longest wavelengths (λ > 1110 nm) entering the SWIR (short wavelength IR, λ > 1400 nm), respectively.

When *in vivo* drug delivery, cell imaging and photothermal therapies have to be imagined, cellular uptake of GNS should be considered. Data collected for the somewhat smaller GNS from LSB (tip-to-tip distance = 60-70 nm)† [12,13] showed that uncoated GNS from LSB were able to enter HeLa cells but they also were proved to be strongly cytotoxic to SH-SY5Y cells, due to the residual double-layer of LSB on their surface.[15,24] Coating with thiolated polymers containing polyethylene glycol (HS-PEG) allowed complete surfactant removal, producing fully biocompatible GNS from LSB, as we have demonstrated on the SH-SY5Y cell line.[24,25] Coated GNS from LSB are not significantly internalized in cells, unless when overcoated with cationic polymers capable of membrane disruption, such as PAH (polyallylamine hydrochloride).[25] The size and shape of nanoparticles are parameters strongly affecting their internalization in cells.[26] The 40-50 nm range is typically considered optimal for cell internalization, although this has been shown for gold nanoparticles with a spherical shape.[27,28] Moreover, spherical gold nanoparticles display a higher cellular uptake than gold nanorods[29,30] while more complex shapes, such as hexapods, show a higher internalization with respect to gold nanocages and nanorods.[31] This leads to the consideration that when nanoparticles with a given shape are examined for the first time regarding their cellular uptake, the interplaying roles of dimensions and shape bring a high degree of unpredictability. On this background, we decided to work on GNS from TX100 having the shape shown in Figure 1 A, and trying shrinking them to smaller dimensions, bringing their DCI to less than 50 nm, as displayed in Figure 1B. Then, we compared the uptake in SH-SY5Y cells of such smaller, shrunk GNS (named s-GNS) with that of the larger and already described GNS from TX100 (l-GNS), whose interaction with this cell line was never reported before. Additional interest in obtaining smaller GNS is found in the literature reporting that blood circulation of nanoparticles is favoured by dimensions between 10 and 50 nm, as larger ones are removed by

the reticuloendothelial system (*e.g.* by liver and spleen)[32-34] and smaller particles by the renal system.[35-37] However, if we work in the perspective of using s-GNS visual tracking by two-photon luminescence (TPL) and of exploiting the s-GNS photothermal response in biological systems, the s-GNS dimensions and their branches aspect ratio have to be such to keep one of their two main LSPRs inside the bio-transparent window. This could be attained in two ways: either i) by reducing all l-GNS dimensions proportionally, thus maintaining in s-GNS an identical branches aspect ratio, or ii) by decreasing the aspect ratio in s-GNS, allowing the 'long' LSPR band to be shifted to the blue enough to enter the bio-transparent window. In this paper, we present a synthesis allowing to obtain shrunk GNS from TX100 with DCI ~ 40 nm, as displayed in Figure 1B. The aspect ratio of the branches decreases according to hypothesis (ii). The 'intermediate' LSPR band shifts to shorter wavelengths, entering the visible range and merging with the 'short' LSPR band at 500-600 nm, but the 'long' LSPR band shifts so much to the blue to position its maximum at 900-1000 nm, as shown by the green spectrum in Figure 1C. The s-GNS were coated with functional PEG thiols bearing differently charged terminal groups. Their internalization in SH-SY5Y cells and the related cytotoxicity on such cells were studied and compared with that of larger l-GNS, whose interaction with these cells was never reported before.

Materials and methods

Materials.

TritonX-100, Tetrachloroauric acid, Sodium borohydride, Ascorbic acid, Silver Nitrate, 7-mercapto-4-methylcoumarin, α-Methoxy-ω-Mercapto polyethylene glycol MW 2000 (HS-PEG), were all purchased from Sigma-Aldrich and used without further purification. Glycerol was purchased from AtsFaar. α-Mercapto-ω-amino polyethylene glycol hydrochloride MW 3000 (HS-PEG-NH_2) was purchased from Rapp Polymere.

Syntheses.

Prior to all syntheses, the glassware was pre-treated with aqua regia for 20 min. The acid mixture was then discarded, the glassware was filled with bidistilled water and sonicated for 3 min. The bidistilled water-sonication cycle was repated 3 times. After that, glassware was dried in an oven at 120 °C.

l-GNS. The synthesis was carried out according our already described general approach,[14] under the following conditions. A seed solution was prepared in a 20mL vial. 5mL of HAuCl4 5×10^{-4}M in water were added to 5mL of an aqueous solution of TX100 0.1M (final TX100 concentration = 0.05M). The mixture was gently hand-shaken until a pale yellow colour appeared. Then 0.60 mL of an ice-cooled solution of $NaBH_4$ 0.01M in water were added and the mixture was gently hand-shaken. A red-brown colour soon appeared. The seed solution was kept in ice and used within 2 hours. The growth solution was prepared in a 20mL vial. 250µL of $AgNO_3$ 0.004M in water and 5mL of $HAuCl_4$ 0.001M in water were added in this order to 5mL of an aqueous solution of TX100 0.1 M (final TX100 concentration = 0.05M). Then, 200µL of an aqueous solution of ascorbic acid 0.0788M were added. When the solution became colourless 12µL of the seed solution were added. The solution was gently hand-shaken, until grey-green colour soon appeared, which then turned to blue. The sample was allowed to equilibrate for 2 hrs at room temperature. These were the colloidal solutions on which all the surface functionalizations were carried out. Inductively Coupled Plasma optical emission spectroscopy analysis (ICP-OES) to determine yield were carried out on ultracentrifuged pellets of these solutions, oxidized with aqua regia, observing ~ 70 % yield (calculated on the basis of total Au).

s-GNS. Shrunk GNS were prepared with an identical procedure, except for the volume of the growth solution and of the added seed solution, that was prepared as described for l-GNS. In particular, in the synthesis that we adopted for the s-GNS used in all characterization and experiments with cells, we added to a 20 mL vial 5.0 mL of bidistilled water containing 0.1M TX100. Then, in sequence, we added 250 µL $AgNO_3$ 0.004 M, 5.0 mL $HAuCl_4$ 0.001M, 200 µL of an aqueous solution of ascorbic acid 0.0788M and 55 µL of seed solution (final TX100 concentration = 0.05 M). In this preparation both seed and growth solutions have the same Au concentration as for l-GNS, but the seed/growth volume ratio (mL/mL) has increased from 0.012/10 (l-GNS) to 0.055/10 (s-GNS). A violet solution was obtained after equilibration for 2 hrs at room temperature. ICP-OES analysis to determine yield were carried out on ultracentrifuged s-GNS pellets from these solutions, oxidized with aqua regia, observing ~ 65 % yield (calculated based on total Au).

Coated l-GNS and s-GNS. Coating with HS-PEG and HS-PEG-NH_2 was carried out according to the described procedure.[14] Briefly, to 10mL of a GNS solution the polymers were added either as solids or from a concentrated aqueous solution, to reach 5×10-5 M concentration. After 2 hours of gentle shaking on a reciprocating stirrer at room temperature, solutions were ultracentrifuged (13000 rpm, 15 min) to eliminate excess PEG and excess TX100. The supernatant was discarded and the obtained pellet was redissolved in 10 mL bidistilled water. The ultracentrifugation/redissolution cycle was repeated two more times to eliminate all the residual TX100.

Methods and Instrumentation

GNS size and Z-potential were measured with a Malvern Zetasizer Nano ZS90 instrument, equipped with a dedicated dip-cell electrode for Z-potential measurements, on 1 mL samples of colloidal solutions.

Absorption spectra were measured on a Cary 50 Varian, instrument (180-1100 nm) or on a Cary 6000 instrument (300-1800 nm) in cells with 1 cm or 1 mL optical path.

Ultracentrifugation was carried out with a Hermle Z366 ultracentrifuge.

Quantitative Au analysis to determine yields was carried out using ICP-OES. Pellets of l-GNS or s-GNS obtained by ultracentrifugation of 2.0 mL of growth solution were treated with 400µL of freshly prepared aqua regia. After the addition of aqua regia immediate oxidation was observed, with decoloration. Each sample was then diluted 1:20 with bidistilled water and analyzed with an ICP-OES OPTIMA 3000 Perkin Elmer instrument.

Conventional Transmission Electron Microscopy (TEM) imaging was carried out with a Jeol JEM-1200 EXII140 instrument, on pegilated solutions of GNS, diluted 1:10 before casting a drop on copper grids coated with parlodion.

High Resolution TEM (HR-TEM) analyses were carried out at KAUST using a FEI Titan microscope, operating at an acceleration voltage of 300 kV, equipped with an ultra-bright Schottky electron source (FEI X-FEG), a super-twin objective lens and a Gatan 2k×2k CCD camera. Seeds solution was ultracentrifuged once, the supernatant discarded and the pellet redissolved in the same amount of bidistilled water. Grids were prepared by dropcasting after 1:10 dilution. GNS solutions were first coated with PEG-SH as described, then ultracentrifuged, the supernatant discarded and the pellet redissolved in the same volume of bidistilled water. Dropcasting was then carried out on 1:10 diluted solutions. Both seeds and GNS were deposited on copper grids coated with an ultrathin amorphous carbon film.

The photothermal response of the s-GNS solutions was examined when primed by the 800-920 nm output (collimated 1.2 mm waist) of a tunable NIR laser (MaiTai Spectra Physics, CA), working in continuous wave, with 50-400 mW power. Temperature was measured using a ThermaCAM SC 3000 (FLIR Systems) camera (320x240 microbolometers array) operating in the spectral range of 8-9 µm, numerical aperture NA = 0.46 x 0.34. The acquisition frequency is 9 Hz with a sensitivity of 0.1°C and an accuracy of ±0.2°C. For direct measurements of the temperature increase of GNS solution under irradiation, 1 mL solution of s-GNS coated with HS-PEG-NH_2 (10x concentration) was placed in plastic wells (Nunc, Labtek, D) and irradiated by laser. The thermocamera was placed at a distance of 0.5 m from the sample. Temperature was measured until a plateau was reached (typically in 10-15 min). The temperature as a function of time was obtained from a region of interest (ROI) selected on the thermal image and recorded with a dedicated program.

Studies on cells

Cell culture and treatments. SH-SY5Y human neuroblastoma cell line was purchased from the American Type Culture Collection (ATCC, Manassas, VA, USA). The cells were grown in Eagle's minimum essential medium supplemented with 10% fetal bovine serum, 1% penicillin-streptomycin, L-glutamine (2 mM), non-essential amino acids (1 mM), and sodium pyruvate (1 mM) at 37 °C, in an atmosphere of 5% CO_2 and 95% humidity. [38] Cells were treated for 4, 24 or 48 hrs with different concentrations of l-GNS and s-GNS coated with HS-PEG_{2000} and HS-PEG-NH_2.

MTT assay. Mitochondrial enzymatic activity was estimated by the MTT [3-(4,5-dimethylthiazol-2-yl)-2,5-diphenyltetrazolium bromide] assay (Sigma-Aldrich, Milan, Italy). A cell suspension of 10,000 cells/well in 100 μL culture medium was seeded into 96-well plates. After each treatment with GNS (4, 24 and 48 hrs, with different Au concentration), the medium was substituted with fresh one and then 10 μL of MTT (final concentration equal to 1 mg/mL) was added to each well. After incubation at 37°C for 4 hrs, the formed purple formazan crystals were solubilized in 100 μL of lysis buffer (20% sodium dodecyl sulphate in 50% dimethylformamide) overnight at 37°C. Absorbance values were measured at 595 nm in a microplate reader (SynergyHT, BioTek Instruments, Inc.) and the results expressed as % with respect to the control value (100%).

Two-photon luminescence microscopy and cellular uptake. Cells were processed according to Marchesi et al. [39] with minor modifications. Briefly, cells plated (80,000/well) on glass coverslips (22x22 mm), were treated for 48 hrs with 25 μg/mL of s-GNS and l-GNS coated either with HS-PEG and HS-PEG-NH2. After treatments, cells were washed with Phosphate-buffered saline (PBS), fixed for 20 min in 70% ethanol at −20 ◦C, washed again with PBS and permeabilized for 15 min at room temperature with 0.1% TX100 in PBS. Cells were then washed with PBS and, to visualize the nucleus, stained for DNA for 5 min with a solution of 0.1 μg/ml Hoechst 33342.

Finally, the cells were imaged with a custom-modified two-photon laser scanning system. Two photon excitation at 800 nm was exploited, with an average excitation power of 20 mW, measured before the entrance pupil of the 25x 1.05NA objective (Olympus). The GNS TPL emission was selected by a band-pass filter (Chroma Inc., Brattelboro, VT, HQ535/50) centered at 535 nm, while the fluorescence signal from Hoechst 33342 was discriminated by a 460/20nm band-pass filter (Chroma Inc., Brattelboro, VT, HQ460/20). Images shown in this article are the result of 3 Kalman average scans; 10-14 z planes were acquired along the z axis at 1.0 μm inter-distance.

Internalization of GNS. SH-SY5Y cells plated (300,000/well) on a 6-well plate, were treated for 48 hrs with 25 μg/mL s GNS and l-GNS solutions, coated with HS-PEG and HS-PEG-NH2 (2.9 mL volume added in each well). After treatments, cells were washed 3 times with PBS, and then treated with Cell Lysis Buffer 1X (Cell Signaling) for 5 min to lyse the cells under non-denaturing conditions. The cell lysate was transferred into an eppendorf tube and ultracentrifuged (13000 rpm for 10 min). The pellet was separated from the supernatant and treated with 500 μL of freshly prepared aqua regia. After 16 hrs of incubation at room temperature the samples were diluted to 3 mL with bidistilled water and analyzed for the Au content with ICP-OES.

Results and Discussion

Synthesis. All the synthetic parameters were kept identical for l-GNS and their shrunk version, except for the seeds concentration in the growth solution. The seeds solution was the same for all syntheses, with 2.358×10^{-4} M Au concentration. Since we use an excess of $NaBH_4$ to prepare seeds from $[AuCl_4]^-$, we confidently assume that all Au(III) is reduced to elemental gold. The average dimensions of the seeds can be calculated by their HR-TEM imaging. Although the seeds were hard to image due to the presence of an excess of surfactant, which decomposing under the electron beam gave fast rise to an external carbon layer growth which covered the seeds, heavily affecting the final quality of the HR-TEM images, they appear as polycrystalline spherical objects (see ESI S1). From the images, an average 3.6(0.5) nm diameter was determined.

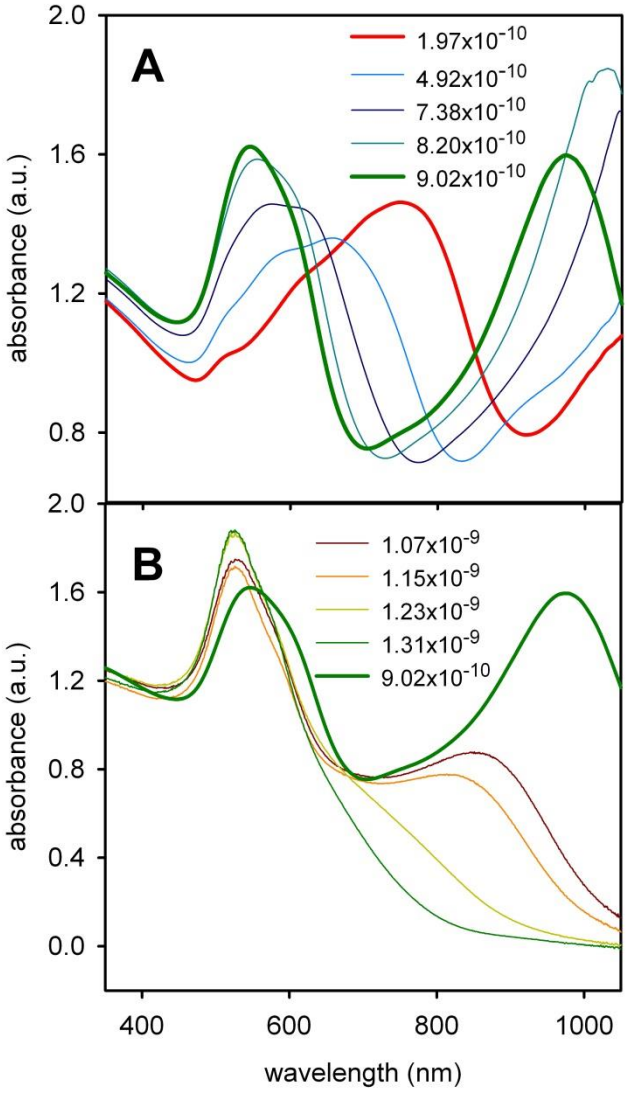

Figure 2. A: Series of absorption spectra for seeds concentration in the growth solution from 1.97×10^{-10} M (thick red spectrum = l-GNS) to 9.02×10^{-10} M (thick green spectrum = s-GNS). **B:** same, for concentrations 9.02×10^{-10} M to 1.07×10^{-9} M. The thick green spectrum at 9.02×10^{-10} M (s-GNS) is the same of panel A, reproduced in panel B for sake of clarity. All the concentrations and corresponding colours are depicted in the figure

By this, using the elemental Au density (19320 kg/m³), the seeds concentration in their solution could be calculated, obtaining 1.64×10^{-7} M (*i.e.* mol of seed nanoparticles/L). It has to be pointed out that this is the same concentration of the gold seeds solutions used in all our previously described syntheses in TX100, which led to l-GNS. We first replicated such syntheses using an already tested set of conditions[14] for the growth solution, i.e. given concentrations of TX100, $[AuCl_4]^-$, ascorbic acid, silver nitrate and added seeds (see Experimental). In particular, to obtain l-GNS the concentration of the seeds in the growth solution was 1.97×10^{-10} M. We have reported that such a set of conditions led to 5-branched l-GNS with 70-80 nm DCI and an intermediate LSPR band at 750 nm.

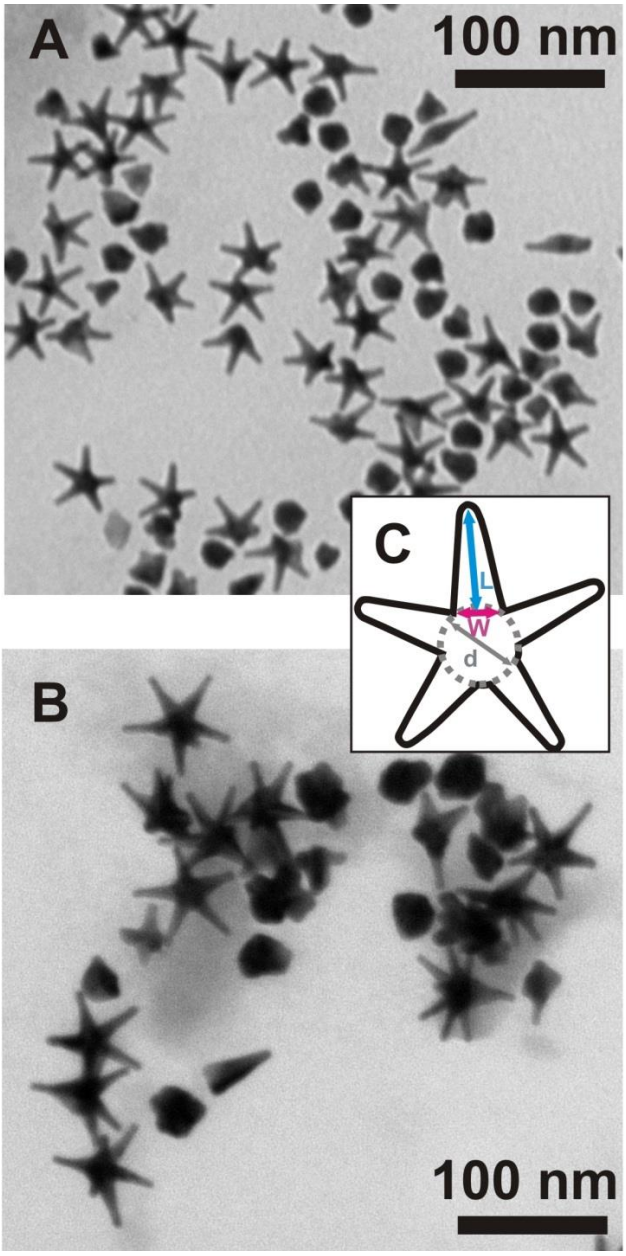

Figure 3. **A**: TEM image of s-GNS; **B**: TEM image of l-GNS; **C**: geometrical schematization of GNS: branch length (L), branch width (W) and core diameter (d)

Figure 2A, red thick line, displays the absorption spectrum of the product that we obtained in this study, that agrees with our previous literature. Figure 3B displays a TEM image of this l-GNS, while Figure 1C reports also their full 400-1800 nm absorption spectrum (red line), displaying the long LSPR band at 1300 nm. Then we progressively increased the volume of the seeds solution added to the growth one, exploring the 1.97×10^{-10} - 1.31×10^{-9} M seeds concentration range in the growth solution. For sake of visual clarity, Figure 2A displays the absorption spectra obtained for the 1.97×10^{-10} – 9.02×10^{-10} M concentration range and Figure 2B for the 9.02×10^{-10} - 1.31×10^{-9} M range. In Figure 2A, on increasing the seeds concentration in the growth solution the maximum of the intermediate LSPR band shifts from 750 nm (l-GNS, thick red spectrum) to ~ 650 nm (thick green spectrum), appearing as a shoulder of the LSPR short band (λ_{max} = 542 nm), that increases in intensity. On the other hand, the long LSPR band shifts from the SWIR range to the NIR, entering as expected the biotransparent range. λ_{max} is 1300 nm at 1.97×10^{-10} M seeds concentration (l-GNS, red

thick spectrum, maximum out of range in Figure 2A,) and it is found at 970 nm for 9.02×10^{-10} M seeds concentration (green thick spectrum). As it can be seen in Figure 2B, further increase of the seeds concentration in the growth solution leads to the further blue shift of the long LSPR band, but with a significant decrease of its intensity, observing its disappearance at high seeds concentrations. To our aims, the best compromise is obtained with 9.02×10^{-10} M seeds concentration, green thick spectrum in Figure 2A and 2B. For all the successive experiments and characterizations, we used the nanoparticles synthesized under such conditions, which are the species that we named s-GNS. The TEM image of s-GNS displayed in Figure 3A allows the direct visualization of the effective shrinking of s-GNS with respect to l-GNS (Figure 3B). Average DCI is 76 nm and 46 nm for l-GNS and s-GNS, respectively, with a ~ 40% decrease. The change in the absorption spectrum is due to the decrease of the aspect ratio of the GNS branches (L/W, Figure 3C for L and W definition), changing from 2.5 to 2.0 on passing from l-GNS to s-GNS.

Table 1. Dimensional parameters (nm) of the studied nanoparticles, obtained from TEM images. Standard deviation in parenthesis.

	l-GNS[a]	s-GNS[b]	excess seeds[c]
length	27.8 (3.6)	15.8 (2.5)	13.3(2.8)
base	11.0 (1.6)	7.9 (1.2)	8.0(1.5)
aspect ratio[d]	2.5	2.0	1.7
core (d)	20.7 (1.5)	14.9 (1.6)	15.4 (1.3)
% GNS	57%	38%	12%
DMI	76 (3.5)	46 (2.2)	-

[a]Seeds concentration in the growth solution = 1.97×10^{-10} M; [b] seeds concentration in the growth solution = 9.02×10^{-10} M; [c] seeds concentration in the growth solution = 1.23×10^{-9} M; [d]calculated as the ratio between average length and average base values

Table 1 reports the relevant dimensional parameters for both species (see ESI S2 for full TEM images). The increased absorption of the ~ 550 nm band in s-GNS with respect to l-GNS can be accounted for counting the undeveloped spherical particles in the TEM images (ESI S2). Data summarized in Table 1 show that the % of spheres increases on increasing the seeds concentration in the growth solution, reaching > 90% at the highest seeds concentration. The seed-growth process is often described as a deposition of Au(0) atoms catalyzed by the seeds addition to a solution in which Au(III) has already been reduced to Au(I) by ascorbic acid.[40-44] The surfactant acts as a coating and directing agent, adhering preferentially to the highest energy faces of the nanocrystals and allowing Au(0) deposition on the less efficiently coated faces.[13] Increasing the concentration of seeds, with no changes of the Au(I) quantity in the growth solution, is obviously expected to produce more objects with smaller overall dimensions, as the nucleation centres are more abundant for the same quantity of gold to be reduced. However, to explain the aspect ratio decrease of the branches, the relative variation of the dimensional parameters should be considered. The average length of the branches (L, Figure 3C) changes from 27.8 nm to 15.8 nm from l-GNS to s-GNS, with a 43% decrease. The base width (W, Figure 3C) changes instead from 11.0 nm to 7.9 nm from l-GNS to s-GNS, with a 28% decrease, that is also the same % decrease of the core diameter (d, Figure 3C). The data from TEM images reported in Table 1 show also that the core in the s-GNS and the diameter of the undeveloped spheres are much larger than the seeds dimensions (d < 4 nm). Moreover, examination of HR-TEM images (vide infra) reveals a crystalline domain in correspondence of the GNS centre, from which a second different domain grows, from which the branches develop. We can thus hypothesize a fast non selective growth of the cores followed by a slower branches development process, taking place on preferential crystal faces of large spheroidal objects. When the seeds concentration is too large, spheres predominates or are the only obtained

product, as they are rapidly formed and consume all the Au(I). As an example (Table 1), when 1.23×10^{-9} M seeds concentration is used, spheroids are 88%, with a 17.3(1.6) nm diameter. In the few formed GNS the aspect ratio is further decreased to 1.7.

TPL and photothermal response. The two-photon excitation spectrum has been recorded by irradiating a s-GNS solution with a femtosecond pulsed laser in the NIR 730-920 nm range and collecting the emission of s-GNS at 480 and 535 nm. As observed for l-GNS[14] and GNS from LSB,[15] the emission intensity increases with wavelength in the examined range (see ESI S3A), following the profile of the absorption spectrum (ESI S3B) that is shown in Figure 2A and B (green thick line). This is in full agreement with the typical behaviour expected for two-photon luminescence from gold nanoparticles, *i.e.* the intensity of the luminescence emission observed by irradiating at different excitation wavelengths is directly proportional to the LSPR absorbance. [15,45] The photothermal effect was also investigated by recording thermograms, *i.e.* measuring T *vs* time with a thermocamera while irradiating a s-GNS solution with a continuous laser source at different wavelengths (800, 840, 900, 920 nm). We maintained the same laser beam waist (1.2 mm) and changed the power in the 50-400 mW range, at each irradiation wavelength. In all cases, we observed a behaviour similar to what we already reported for GNS both from TX100[13] and from LSB:[12] a steep T increase turning into a plateau after 400-500 s (see ESI S4A and S4B). As we have recently described for GNS from LSB,[15,46] the T *vs* time profile reaches the plateau with a double exponential trend. The faster relaxation component (τ_1) is ascribed to the heat exchange from the s-GNS to water within the irradiated suspension. The slower relaxation component (τ_2) is instead ascribed to the exchange of the solution with the laboratory environment. The values of τ_1 and τ_2 do not change significantly with the irradiation wavelength, oscillating between 20-35 s (τ_1) and 226-282 s (τ_2), see ESI S4C. Moreover, defining ΔT= T(plateau) – T(t = 0), the ΔT *vs* laser power trend is found to increase linearly at any irradiation wavelength, in full agreement with the already reported results[14,15,46], see ESI S4D. The ΔT values measured for s-GNS solutions are consistent with what we have already observed for l-GNS solutions of similar concentration and with analogous laser densities. As an example, irradiation on the maximum absorption of s-GNS (920 nm) gives ΔT ~8 °C at 100 mW laser power, corresponding to 8.8 W/cm^2 power density. We have observed ΔT ~8 °C with l-GNS at the same power density.[14]

HR-TEM imaging. Prior to dropcasting colloidal solutions on grids for HR-TEM characterization, s-GNS were coated with HS-PEG as described in the Experimental, then ultracentrifuged and redissolved in the same amount of bidistilled water. This procedure is needed to eliminate the excess of TX100, which may deteriorate the grid material (ultracentrifugation of non-pegilated GNS gives pellets that cannot be redissolved). Seeds solution can instead be ultracentrifuged as such, and the pellet was redissolved in the same volume of bidistilled water prior to dropcasting. On the other hand, attempts to coat the seeds with HS-PEG and separate them by ultracentrifugation were unsuccessful.

Figure 4A shows the HR-TEM image of one as-synthesized penta-twinned s-GNS. For all the HR-TEM images of GNS, Fourier analysis revealed the reflections expected from the face centered cubic (*fcc)* crystalline structure of gold. In particular, Fig. 4B displays the magnified HR-TEM of one of the six branches belonging to the penta-twinned GNS, corresponding to the larger and dashed red square reported in panel A. On such a branch, in correspondence of the smaller red square, the filtered 2D-Fast Fourier Transform (FFT) was extracted and is reported in upper right panel. Its analysis shows the (111), (200) and (022) lattice sets, having spacing equal to 2.35 Å, 2.03 Å and 1.35 Å, respectively, and corresponding to the [011] zone axis. The arrow indicates the branch growth direction, which was found being the (202) one.

Moreover, as already mentioned in the Results and Discussion Synthesis section, examination of HR-TEM images reveals a crystalline domain in correspondence of the GNS centre, from which a second different domain overgrows, from which the branches develop. The presence of the seed from which the final GNS overgrowth originated could be noticed looking at the central part of HR-TEM image reported in Figure 4A and, for a different value of focus, again in Figure ESI S5. Here, the images of the GNS appear darker and showing roto-translational moiré fringes that can be ascribed to the superposition of two lattice sets coming from different crystalline structures having the same lattice set spacing.

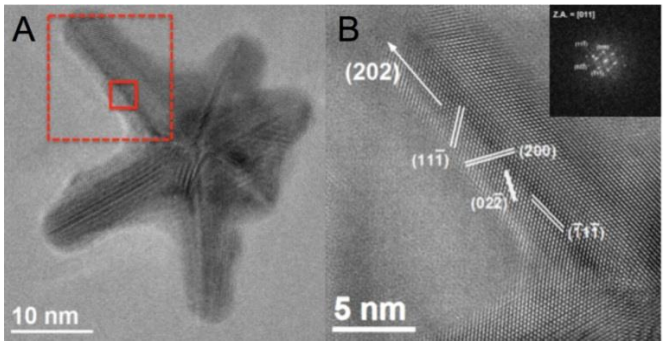

Figure 4. A: HR-TEM image of six-branches of a penta-twinned s-GNS; the larger and dashed square shows the GNS branch imaged at higher magnification and shown in Fig. 4B. The small square indicates the ROI where filtered 2D-FFT, shown in the panel Fig. 4B, was calculated. **B:** (111), (200) and (022) lattice planes of *fcc* gold crystal structure, are displayed. White arrow indicates the (202) growth direction

Interaction with SH-SY5Y cells. SH-SY5Y cells present some advantages: they are able to proliferate for long periods *in vitro* [47] and may be used both in their undifferentiated and differentiated forms.[48] Moreover, they are a valid model for studies that examine neuronal differentiation and metabolism or neurodegenerative disorders.[49] Finally, we have already examined the interactions of the SH-SY5Y cell line with a different but comparable GNS typology, *i.e.* GNS from LSB.[25] Using LSB instead of TX100 as the directing and protecting surfactant, leads to a mixture of monocrystalline and penta-twinned GNS, with the latter prevailing by far.[12,13]

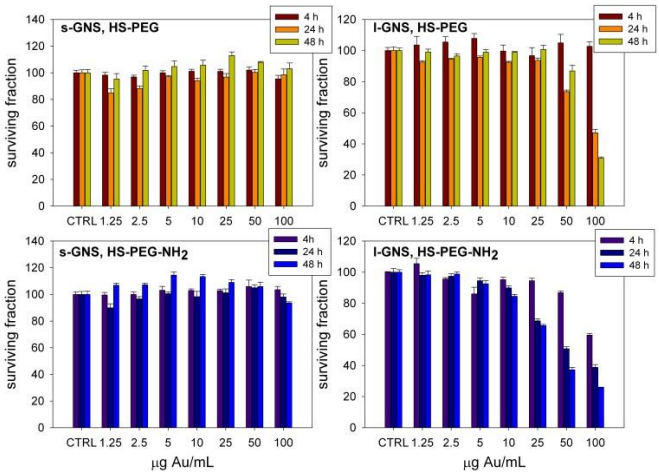

Figure 5. Surviving fractions for SH-SY5Y cells in the presence of s-GNS and l-GNS coated either with HS-PEG (upper row) or HS-PEG-NH_2 (lower row). At each Au concentration three incubation times were studied, 4, 24 and 48 hrs. Colour codes for incubation times, GNS and coating type are indicated in the graphs

Such GNS from LSB have a core with 2-5 protruding branches with a maximum tip-to-tip distance in the 60-70 nm length range.† GNS from LSB were coated with neutral, negatively charged and positively charged PEG coatings. With such coatings biocompatibility tests on SH-SY5Y gave 100% surviving fraction in the 1.25-100 μg Au/mL concentration range, for 4, 24 and 48 hrs incubation time. A reduction of viability (surviving fraction = 50-60%) was observed only at 24 and 48 hrs incubation time and 50-100 μg Au/mL when negatively charged GNS were overcoated with PAH (polyallylamine hydrochloride). The presence of the cationic polymer PAH imparted a highly positive Z-potential to GNS from LSB, which led to an increased GNS internalization, resulting in the deformation of the shape of both cell and nucleus, with membrane disruption.

A positive charge promotes the contact and eventually the internalization of nanoparticles with the negatively charged SH-SY5Y cell membrane.[50,51] On the other hand, in this study we worked on shrunk GNS in order to check the role of small dimensions (DCI< 50 nm) *vs* large dimensions (DCI ~ 80 nm) in

helping GNS internalization in SH-SY5Y cells. In this context, we decided to examine the viability of SH-SY5Y cells in contact with l-GNS and s-GNS from TX100, using HS-PEG as the reference coating and HS-PEG-NH_2 as a positive coating (being protonated at physiological pH 7.4). The cytotoxic PAH overcoating was avoided and negatively charged coatings not examined. It looks noteworthy highlighting that the coating procedure with either HS-PEG or HS-PEG-NH_2 is followed by three cycles of centrifugation, supernatant discard and pellet redissolution in the starting volume of bidistilled water. This allows to eliminate all the surfactant adhering on GNS during the coating procedure.[13] A further final ultracentrifugation cycle was carried out and the pellet redissolved in bidistilled water in 1/10 of the starting volume, in order to obtain concentrated solutions to be used and diluted in the biological experiments (the Au concentration of the concentrated solutions was determined by ICP-OES quantitative analysis prior to use). Z-potential was measured for both GNS types and coatings, finding slightly negative values for both l-GNS and s-GNS with HS-PEG (see Table 2), and positive values at pH 7.5 with HS-PEG-NH_2 coating (+12 and +15 mV for s-GNS and l-GNS at pH 7.5, respectively). A complete picture of the measured Z-potential values is displayed in Table 2. While significant pH-dependence is observed for HS-PEG-NH_2 coating (as a function of the protonation degree), no variation is observed for the neutral HS-PEG coating.

Viability of SH-SY5Y cells was examined with Au concentrations in the 1.25-100 μg Au/mL range, for 4, 24 and 48 hrs incubation times. The results visually displayed in Figure 5 show that while s-GNS are non-cytotoxic at all the examined concentrations and incubation times, while l-GNS might exert a significant cytotoxicity. In the case of l-GNS coated with HS-PEG, a viability reduction to 70-85% is observed at 50 μg Au/mL for 24 and 48 hrs incubation time, while a more evident viability reduction to 48% and 31% is observed at 100 μg Au/mL with 24 hrs and 48 hrs contact time, respectively. At short contact time (4 hrs) no cytotoxicity is observed even at the highest Au concentrations. On the other hand, when using the positively charged HS-PEG-NH_2 coating, a significant reduction in the viability is observed also at 25 μg Au/mL, with larger viability decrease when 50 and 100 μg Au/mL are used (*e.g.* reaching 60, 39 and 26% at 4, 24 and 48 hrs, respectively, with 100 μg Au/L concentration). Moreover, a larger viability decrease with longer incubation times is generally observed at concentrations ≥ 25 μg Au/mL.

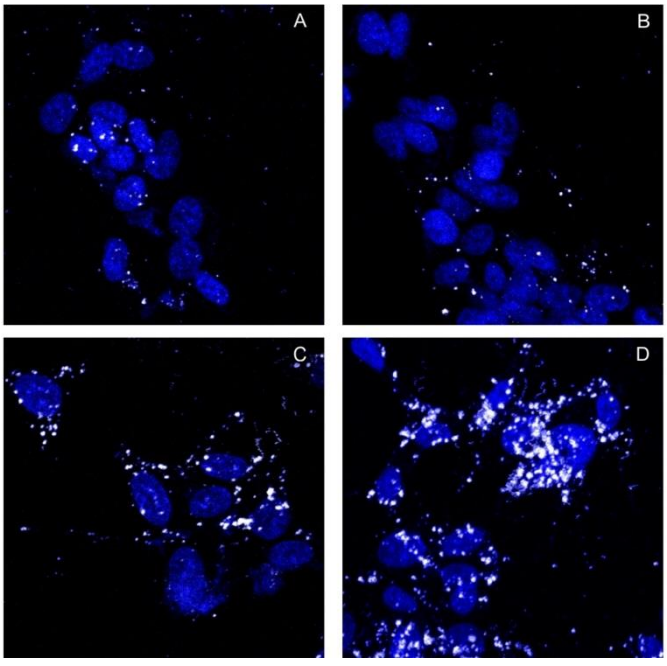

Figure 6. TPL imaging of SH-SY5Y cells treated with GNS at 25 μg Au/mL, with 24 hrs contact time; all images are 1024x1024 pixel, corresponding to 283x283 μm (1 pixel = 276 nm). **A**: treated with s-GNS coated with HS-PEG; **B**; treated with s-GNS coated with HS-PEG-NH_2; **C**: treated with l-GNS coated with HS-PEG; **D**: treated with l-GNS coated with HS-PEG-NH_2

The striking difference between s-GNS and l-GNS correlates with TPL images, obtained exploiting the two-photon luminescence of GNS. Exciting with a femtosecond pulsed laser at 800 nm and using a 535 nm band pass filter allows to visualize GNS emission in white colour, while nuclei are in blue colour thanks to the

Hoechst 33342 fluorescent dye (see Experimental for details). For TPL imaging SH-SY5Y cells were treated in all cases with a concentration of GNS (25 μg Au/L) and contact time (48 hrs) at which we observed complete surviving except when using l-GNS coated with HS-PEG-NH_2. The images show a negligible quantity of s-GNS positioned in the cell area, independently on the coating (see Figure 6 A and B). Such a quantity significantly increases for l-GNS coated with HS-PEG (Figure 6C) while in the case of l-GNS coated with the protonated, positively charged HS-PEG-NH_2 polymer, we observe a striking increase of the l-GNS in the cells area (Figure 6D). The question remains open if the GNS are simply adhering to the membrane, are internalized in the cytoplasm, or are internalized in the nucleus. Examination of single-plane images in our previous work on GNS from LSB indicated that internalization was limited to the cytoplasm and did not occur in the nucleus.[25] Single-plane images of l-GNS coated with HS-PEG and HS-PEG-NH_2 (see ESI S6) suggest that the same holds also in the present work. Moreover, simple adhesion to the SH-SY5Y membrane should be driven by interactions with the external surface of GNS, *i.e.* by their coating and its charge. In the case of s-GNS and l-GNS coated with HS-PEG-NH_2, the nanoparticles surface is identical (see Table 2 for Z-potential values) but a very different quantity of GNS is observed in the cell area in Figure 6B and 6D, also in this case suggesting that l-GNS penetrate into the cytoplasm.

Table 2. Z-potential values of coated GNS and % of internalization

	Z-potential (mv)[a]			% internalized Au[b]
	pH 5.0	pH 7.5	pH 10.0	
s-GNS/HS-PEG	-8	-8	-9	3.3(2.1)
s-GNS/HS-PEG-NH_2	+ 25	+ 15	-2	2.5(1.4)
l-GNS/HS-PEG	-11	-11	-10	6.9 (1.8)
l-GNS/HS-PEG-NH_2	+30	+12	-3	18.4(2.2)

[a]Values averaged on 3-5 different measurements, standard deviation in parenthesis; [b]% value obtained on the basis of the Au found for internalized particles with respect to the total gold added in each well (2 mL at 25 μg Au/mL concentration).

Quantitative determination of Au in cells after incubation of both s-GNS and l-GNS supports what is shown in Figure 6. Table 2 reports the % values of gold found in cells after 48 hrs incubation with 2 mL of GNS, determined after repeated cell washing, cell lyse, separation of the lysate and oxidation with aqua regia for ICP-OES analysis. The highest % values are found for l-GNS coated with HS-PEG-NH_2 (18.4) followed by l-GNS coated with HS-PEG (6.9%). These observations indicate that the larger l-GNS penetrate significantly in SH-SY5Y cells, especially when coated with a positively charged polymer, and that internalization correlates with a decrease of the cells viability. On the other hand, s-GNS do not enter significantly the cytoplasm of the same cells, both with positive or neutral polymer coating. The investigation of the biological mechanism behind this observation is by far out of the goal of the present research. However, as GNS from LSB have demonstrated to be efficient carriers in delivering siRNA to the nucleus of human breast carcinoma cells,[52] optimization of cytoplasm penetration by GNS from TX100 is by itself a relevant step forward in view of future applications. On the other hand, as we have reported in the introduction, the factors affecting the cellular uptake of nanoparticles, such as shape, dimension, coating, overall charge and, of course, the nature of the considered cellular line[26-31] combine in an unpredictable way. While for spherical gold nanoparticles a 40-50 nm diameter is considered optimal for cellular uptake,[27,28] large Au nanohexapods with 60 nm tip-to-tip length and 14 nm branch width were up-taken in MDA-MB-435 cells more efficiently then Au nanorods of 36 nm length and 9 nm width. In this context, the observation that s-GNS (DCI 40 nm) are up-taken by SH-SY5Y cells less than l-GNS (DCI 80 nm) is not surprising.

Conclusions

The increase of the seeds concentration in the growth solution allows to obtain GNS from TX100 that have overall dimensions (DCI) shrunk at ~ 60 % of those obtained with our already published procedure. Careful examination of the HR-TEM GNS imaging reveals that a crystalline domain forms from the seeds in

correspondence of the GNS centre, from which a second different domain grows, where branches develop. The first process is faster, thus consuming a large quantity of Au and leading to GNS with short and large branches. The decreased branches aspect ratio leads in turn to the blue shift of both the NIR LSPR of the GNS. In s-GNS one LSPR reaches the visible range, while the second is still centered in the NIR with λ_{max} = 970 nm and a high absorption also in the biotransparent window. This would in principle allow hyperthermal treatments with s-GNS, as we have demonstrated irradiating their colloidal solutions in the 800-900 nm range and obtaining a strong thermal response. Moreover, the NIR LSPR absorption also allows to obtain a fluorescent signal from s-GNS with the TPL technique, by irradiating in the same range. Thanks to TPL imaging and ICP-OES measurements we have been able to understand that larger GNS (l-GNS) are better internalized in SH-SY5Y cells than s-GNS. The internalization correlates with a decrease in the cells viability. It has to be noticed that the most abundant GNS internalization is observed for nanoparticles with ~ 80 nm overall dimensions (DCI). Smaller ones (DCI 40-50 nm) are poorly internalized, despite the dimensional interval often indicated in the literature as the optimal one[26-28] for spherical gold nanoparticls. This observation adds a further indication that dimensions surely play a fundamental role in the nanoparticles/cells take up processes but also that conclusions obtained for a given shape could be useless for nanoparticles of the same material but with a dramatically different shape.[29-31]

Acknowledgements

This work was supported by the Italian Ministry of Instruction, University and Research (MIUR) and by PRIN 2010–11 [20109PLMH2]. The University of Pavia and CIRCMSB (Consorzio Interuniversitario di Ricerca in Chimica dei Metalli nei Sistemi Biologici) are also gratefully acknowledged for support. LD would like to thank Sara Oprandi for her help in collecting the photothermal response data.

Notes and references

† GNS from LSB have a core with 2-5 protruding branches that are shorter and larger than in GNS from TX100. Moreover, GNS from LSB do not have a regular shape and graphical inscription into a circumference is impossible. Instead of DCI the maximum tip-to-tip distance was used to evaluate their overall dimensions, with values in the 60-70 nm range.

1 A. Guerrero-Martínez, S. Barbosa, I. Pastoriza-Santos and L.M. Liz-Marzán, *Curr. Opin. Colloid Interface Sci.*, 2011, **16**, 118–127. DOI:10.1016/j.cocis.2010.12.007

2 M. Yamamoto, Y. Kashiwagi, T. Sakata, H. Mori and M. Nakamoto, *Chem. Mater.*, 2005, **17**, 5391–5393. DOI: 10.1021/cm0515000

3 G. C. Khoury and T. Vo-Dinh, *J. Phys. Chem. C*, 2008, **112**, 18849–18859 DOI: 10.1021/jp911355q

4 P. S. Kumar, I. Pastoriza-Santos, B. Rodriguez- Gonzalez, F. J. Garcia de Abajo and L. M. Liz-Marzan, *Nanotechnology*, 2008, **19**, 015606 DOI: 10.1088/0957-4484/19/01/015606

5 S. Chen, Z. Lin Wang, J. Ballato, S. H. Foulger and D. L. Carroll, *J. Am. Chem. Soc.*, 2003, **125**, 16186–16187. DOI: 10.1021/ja038927x

6 T. K. Sau and C. J. Murphy, *J. Am. Chem. Soc.*, 2004, **126**, 8648–8649. DOI: 10.1021/ja047846d

7 E. Hao, R. C. Bailey, G. C. Schatz, J. T. Hupp and S. Li, *Nano Lett.*, 2004, **4**, 327–330. DOI: 10.1021/nl0351542

8 W. Ahmed, E. S. Kooij, A. van Silfhout and B. Poelsema, *Nanotechnology*, 2010, **21**, 125605. DOI:10.1088/0957-4484/21/12/125605

9 G. Kawamura and N. Nogami, *J. Cryst. Growth*, 2009, **311**, 4462–4466. DOI:10.1016/j.jcrysgro.2009.08.002

10 G. Kawamura, Y. Yang, K. Fukuda and M. Nogami, *Mater. Chem. Phys.*, 2009, **115**, 229-234. DOI: 10.1016/j.matchemphys.2008.11.064

11 C. L. Nehl and J. H. Hafner, *J. Mater. Chem.*, 2008, **18**, 2415–2419. DOI: 10.1039/b714950f

12 P. Pallavicini, G. Chirico, M, Collini, G. Dacarro, A. Donà, L. D'Alfonso, A. Falqui, Y.A. Diaz-Fernandez, S. Freddi, B. Garofalo, A. Genovese, L. Sironi, and A. Taglietti, *Chem. Commun.*, 2011, **47**, 1315-1317. DOI: 10.1039/c0cc02682d

13 A. Casu, E. Cabrini, A. Donà, A. Falqui, Y. Diaz-Fernandez, C. Milanese, A. Taglietti, and P. Pallavicini, *Chemistry Eur J.*, 2012, **18**, 9381-9390. DOI: 10.1002/chem.201201024

14 P. Pallavicini, A. Donà, A. Casu, G. Chirico, M. Collini, G. Dacarro, A. Falqui, C. Milanese, L. Sironi, and A. Taglietti, *Chem. Commun.*, 2013, **49**, 6265-6267. DOI: 10.1039/c3cc42999g

15 L. Sironi, S. Freddi, M. Caccia, P. Pozzi, L. Rossetti, P. Pallavicini, A. Donà, E. Cabrini, M. Gualtieri, I. Rivolta, A. Panariti, L. D'Alfonso, M. Collini, and G. Chirico, *J. Phys. Chem C*, 2012, **116**, 18407−18418. DOI: 10.1021/jp305021k |

16 A. Shiohara, Y.S. Wang, L.M. Liz-Marzan, *J. Photochem. Photobiol. C*, 2014, **21**, 2-25. DOI: 10.1016/j.jphotochemrev.2014.09.001

17 Y. Liu, H. Yuan, F.R. Kersey, J. K. Register, M. C. Parrott, and T. Vo-Dinh, *Sensors*, 2015, **15**, 3706-3720. DOI: 10.3390/s150203706

18 G. Chirico, P. Pallavicini and M. Collini, *Nanomedicine*, 2014, **9**, 1-3. DOI: 10.2217/nnm.13.186

19 P. Pallavicini, A. Donà, A. Taglietti, P. Minzioni, M. Patrini, G. Dacarro, G. Chirico, L. Sironi, N. Bloise, L. Visai, and L. Scarabelli, *Chem. Commun.*, 2014, **50**, 1969-1971. DOI: 10.1039/c3cc48667b

20 P. Pallavicini, S. Basile, G. Chirico, G. Dacarro, L. D'Alfonso, A. Donà, M. Patrini, A. Falqui, L. Sironi and A. Taglietti, *Chem. Commun.*, 2015, **51**, 12928-12930.

21 S. Link and M. A. El-Sayed, *J. Phys. Chem. B*, 1999, **103**, 8410–8426. DOI: 10.1021/jp9917648

22 M. Quinten and U. Kreibig, *Surf. Sci.*, 1986, **172**, 557. DOI: 10.1016/0039-6028(86)90501-7

23 R. Weissleder, *Nat. Biotechnol.*, 2001, **19**, 316-317. DOI: 10.1038/86684

24 G. Cavallaro, D. Triolo, M. Licciardi, G. Giammona, G. Chirico, L. Sironi, G. Dacarro, A. Donà, C. Milanese, and P. Pallavicini, *Biomacromolecules*, 2013, **14**, 4260-4270. DOI: 10.1021/bm401130z

25 P. Pallavicini, E. Cabrini, G. Cavallaro, G. Chirico, M. Collini, L. D'Alfonso, G. Dacarro, A. Donà, N. Marchesi, C. Milanese, A. Pascale, L. Sironi, A. Taglietti, *J. Inorg. Biochem.* 2015, **151**, 123–131. DOI: 10.1016/j.jinorgbio.2015.05.002

26 J. Li, H. Mao, N. Kawazoe and G. Chen, *Biomater. Sci.*, 2017, **5**, 173-189. DOI: 10.1039/C6BM00714G

27 B. D. Chithrani A. A. Ghazani and W. C. W. Chan, *Nano Lett.* 2006, **6**, 662-668. DOI: 10.1021/nl052396o

28 B. D. Chithrani and W. C. Chan, *Nano Lett.*, 2007, **7**, 1542–1550. DOI: 10.1021/nl070363y

29 A. Malugin and H. Ghandehari, *J. Appl. Toxicol.*, 2010, **30**, 212–217. DOI: 10.1002/jat.1486

30 M. Janát-Amsbury, A. Ray, C. Peterson and H. Ghandehari, *Eur. J. Pharm. Biopharm.*, 2011, **77**, 417–423. DOI: 10.1016/j.ejpb.2010.11.010

31 Y. Wang, K. C. Black, H. Luehmann, W. Li, Y. Zhang, X. Cai, D. Wan, S.-Y. Liu, M. Li, P. Kim, Z.-Y. Li, L. V. Wang, Y. Liu and Y. Xia, *ACS Nano*, 2013, **7**, 2068-2077. DOI: 10.1021/nn304332s

32 H. Soo Choi, W. Liu, P. Misra, E. Tanaka, J.P. Zimmer, B. Itty Ipe, M.G. Bawendi, J.V. Frangioni, *Nat. Biotechnol*. 2007, **25**, 1165–1170. DOI: 10.1038/nbt1340

33 W. Jiang, B.Y.S. Kim, J.T. Rutka, W.C.W. Chan, *Nat. Nanotechnol.* 2008, **3**, 145–150. DOI: 10.1038/nnano.2008.30

34 H. Gao, W. Shi, L.B. Freund, *Proc. Natl. Acad. Sci. U.S.A.* 2005,**102**, 9469–9474. DOI: 10.1073/pnas.0503879102

35 F. Osaki, T. Kanamori, S. Sando, T. Sera, Y. Aoyama, *J. Am.Chem. Soc.* 2004, **126**, 6520–6521. DOI: 10.1021/ja048792a

36 E. Sadauskas, H. Wallin, M. Stoltenberg, U. Vogel, P. Doering, A. Larsen, G. Danscher, *Part. Fibre Toxicol.* 2007, **4**, 10–17. DOI: 10.1186/1743-8977-4-10

37 W.H. De Jong, W.I. Hagens, P. Krystek, M.C. Burger, A. Sips, R.E. Geertsma, *Biomaterials*, 2008, **29**, 1912–1919. DOI: 10.1016/j.biomaterials.2007.12.037

38 N. Marchesi, C. Osera, L. Fassina, M. Amadio, F. Angeletti, M. Morini, G. Magenes, L. Venturini, M. Biggiogera, G. Ricevuti, S. Govoni, S. Caorsi, A. Pascale, and S. Comincini, *J. Cell. Physiol.*, 2014, **229**, 1776-1786. DOI: 10.1002/jcp.24631

39 N. Marchesi, M. Amadio, C. Colombrita, S. Govoni, A. Ratti, and A. Pascale, *J Alzheimers Dis.*, 2016, **54**, 535-547. DOI: 10.3233/JAD-160299

40 B. Nikoobakht, and M. A. El-Sayed, *Chem. Mater*. 2003, **15**, 1957 – 1962. DOI: 10.1021/cm020732l

41 N. R. Jana, L. Gearheart, and C. J. Murphy, *Chem. Commun.* **2001**, 617 – 618. DOI: 10.1039/B100521I

42 N. R. Jana, L. Gearheart, and C. J. Murphy, *J. Phys. Chem. B* 2001, **105**, 4065 – 4067. DOI: 10.1021/jp0107964

43 N. R. Jana, L. Gearheart, and C. J. Murphy, *Adv. Mater.* 2001, **13**, 1389 –1393. DOI: 10.1002/1521-4095(200109)13:18<1389::AID-ADMA1389>3.0.CO;2-F

44 B. Nikoobakht, and M. A. El-Sayed, *Langmuir* 2001, **17**, 6368- 6374. DOI: 10.1021/la010530o

45 H.F. Wang, T.B. Huff, D.A. Zweifel, W. He, P.S. Low, A. Wei, and J.X. Cheng, *P. Natl. Acad. Sci. USA*, 2005, **102**, 15752-15756. 10.1111/j.1751-1097.2008.00507.x

46 M. Borzenkov, G. Chirico , L. D'Alfonso , L. Sironi, M. Collini, E. Cabrini, G. Dacarro, C. Milanese, P. Pallavicini, A. Taglietti, C. Bernhard, and F. Denat, *Langmuir*, 2015, **31**, 8081-8091. DOI: 10.1021/acs.langmuir.5b01473

47 G. Nicolini, M. Miloso, C. Zoia, A. Di Silvestro, G. Cavaletti, and G. Tredici, *Anticancer Res.* 1998, **18**, 2477-2481

48 J. Kovalevich, and D. Langford, in: S. Amini, M.K. White (Eds.), *Neuronal Cell Culture, Methods and Protocols*, vol. 1078, Humana Press, New York 2013, pp. 9–21. ISBN: 978-1-62703-639-9

49 H.R. Xie, L.S. Hu, G.Y. Li, *Chin. Med. J. (Engl.)* 2010, **123**, 1086-1092. DOI: 10.3760/cma.j.issn.0366-6999.2010.08.021
50 A.M. Alkilani and C.J. Murphy, *J. Nanoparticle Res.* 2010, **12**, 2313-2333. DOI: 10.1007/s11051-010-9911-8
51 E.C. Cho, J. Xie, P.A. Wurm and Y. Xia, *Nano Lett.* 2009, **9**, 1080-1084. DOI: 10.1021/nl803487r
52 C. Sardo, B. Bassi, E. F. Craparo, C. Scialabba, E. Cabrini, G. Dacarro, A. D'Agostino, A. Taglietti, G. Giammona, P. Pallavicini, and G. Cavallaro, *Int. J. Pharmaceut.* 2017, **519**, 113-124. DOI: 10.1016/j.ijpharm.2017.01.022

7: Electronic Supplementary Material

Click here to download 7: Electronic Supplementary Material: ESI.pdf